

Design of a Composite Adaptive Controller For the Single-axis 2-DOF MEMS Vibratory Gyroscope with the Competency Of Rotation Rate Measurement

Ehsan Ranjbar*, Amir Abolfazl Suratgar**

* *Research Assistant, MEMS Dynamics & Control Research Group (e-mail: en.ranjbar.eeng@gmail.com).*

** *Assoc. Prof., Industrial Control Lab, Dept. of Elec. Eng., Amirkabir University of Technology, 424, Hafez Ave, Tehran, Iran (e-mail: a-suratgar@aut.ac.ir)*

Abstract: The paper contributes a special design of a 2-DOF MEMS (Micro Electro Mechanical System) vibratory gyroscope in a mere schematic way which has benefit of being manipulated by balanced force actuation mechanism and a differential capacitive sensing one as well. These two embedded mechanisms function along drive and sense axes because the control-task system requires observation of displacement and velocity states simultaneously. In other significant stand, a composite adaptive controller (CAC) is suggested to hold quadrature error compensation true compelling the sensory oscillation mechanism to get vibrated with distinct frequency and amplitude in a sinusoidal manner. Not only does the proposed composite scheme takes advantage of rotation rate estimation being subjected to persistent excitation, but also it gains the benefit of rapid tunable estimation, considerable identification sharpness and an intrinsic adjustable structural robustness in comparison to the adaptive sliding mode controller (ASMC). The simulation results emerge persuasive. It is worthwhile being mentioned that quadrature error and uncertainty get significant in fabrication procedures and ruin sense mode gyroscope response. They mainly originate from slight geometrical distortion which itself causes aniso-damping and aniso-elasticity. Furthermore, inaccuracy in modeling and fabrication process necessitates design of an effective controller. Tracking performance shortcomings in pole-placement state-feedback controller and integral rotation rate estimation requires considering other modern controllers such as adaptive ones.

Keywords: MEMS, gyro, 2-DOF, composite adaptive control, rapid estimation, robustness.

1. INTRODUCTION

MEMS vibratory gyroscope sensors are exploited for angular rotation rate measurement at a large group of rotary machines due to their extraordinary benefits and distinctions. The most basic MEMS vibratory gyroscope is a 2-DOF gyro which is comprised of a suspended seismic mass - on a silicon substrate. The mass oscillates along drive direction. Being subjected into rotation around z axis, a Coriolis force with the same drive frequency will be induced over the seismic mass in a sinusoidal manner having it vibrate along the y direction (Acar and Shkel, 2008). A practical model is displayed on (Acar and Shkel, 2008). (Rashed and Momeni, 2007) achieved major equations of MEMS gyroscopes with focus on vibratory type and its mechanical parameters. (Fei and Batur, 2009) also derived the dynamical model of a 2-DOF MEMS vibratory gyroscope sensor. The basic design and other modern constructed MEMS gyros in (Acar and Shkel, 2008) lack balanced force actuation mechanisms and also differential capacitance measurement bridges along both drive and sense axes, all functioning simultaneously.

They drastically have effect on sensor linearity and stability particularly utilizing control systems instead of exploitation of resonance frequency lock technique. The progressive schemes have dramatically ameliorated robustness against amplitude variation because of regional frequency shift; however, it requires proposal of control systems to buffer either robustness in a narrower frequency domain or against very small Hertz-to-Hertz frequency variation.

The sense mode vibration along the axis betokens rotation rate into which the gyro is subjected. Considering a controller which guarantees perfect tracking of desired sinusoidal oscillations along the directions with desired amplitudes and frequencies, despite uncertain gyro parameters, is important to realize accurate rotation rate measurement. Adaptive sliding mode control is an effective technique to deal with gradual parameter alteration or control a system with parametric uncertainty with a disturbance rejection capability (Rossomando et al., 2014; Sefriti et al., 2012; Devaraj 2015). Adopting composite adaptive control is a useful solution to attain both aims including parameter estimation. Composite

adaptive control has the benefit of both parameter estimation and adaptive control capability. Various control algorithms are used to exploit vibrational mechatronic systems in an efficient manner. Numerous control solutions have been maintained controlling micro devices, especially MEMS inertial sensors, in recent years (Fei et al., 2013; Juan and Fei, 2013; Wu and Fei, 2016). (Raman et al., 2009) evolved a closed-loop digitally controlled MEMS z-axis gyroscope exploiting unconstrained sigma-delta force balanced feedback control. (Dong and Avanesian, 2009) proposed a modern design methodology and hardware implementation for drive-mode control of vibratory MEMS z-axis gyroscopes utilizing active disturbance rejection control (ADRC) strategy. (Li et al., 2010) presented a nonlinear robust adaptive controller to manage drive axis vibrations in a MEMS z-axis gyro vulnerable to parametric uncertainty and external disturbances. He accomplished it exploiting combination of Dynamic Surface Control (DSC) technique with disturbance attenuation method. (Wang et al., 2011) suggested a frequency control design established upon phase locked loop (PLL). (Saif et al., 2011) proposed a modern technique to approximate time-varying rotation rate utilizing sliding mode observer as well as a robust control scheme for z-axis MEMS gyro performance improvement, in spite of coupling between vibratory gyroscope modes and innate model uncertainties. Terminal Sliding Mode Control (TSMC) was employed to evolve tracking performance of drive and sense modes regarding uncertain model of vibratory gyro. (Fei et al., 2011) proposed a direct adaptive fuzzy control exploiting a supervisory compensation for tracking robustification in a z-axis MEMS gyro. (Jiang et al., 2012) proposed a signal processing method to ameliorate rotation rate sharpness in the gyroscopic system through combining outputs of an array of MEMS gyros. (Salah et al., 2010) adopted a strategic nonlinear estimation method to hold a correct read-out of time-dependant rotation rate exploiting an on-line control-observation scheme. Yuan et al. (2016) contributed algorithmic novelty in parameter estimation at 3-DOF gyros to predominantly manage their stochastic errors and to improve estimation accuracy in an array of gyros.

This article conceptually contributes a schematic design which takes advantage of owning force-balanced electrostatic actuation mechanisms along both x and y axes. The design compels the system to be manipulated and physically controlled in a dramatic way. It shows quite beneficial a schematic design armed with two embedded differential capacitance measuring bridges bringing a physically-observable design at the access. The main accomplishments in comb-drives are long-stroke actuation competency and capability to generate displacement

independent forces, which puts greatly stable actuation mechanism at the access (Acar and Shkel, 2008). The balanced comb drive owns all mentioned extra paramount features and exclusively functions applied voltage linearly. Differential capacitance sensing bridge is normally exploited to make capacitance change with deflection linear. The capacitance alteration inversely turns proportional to the square of the initial gap and sensor performance (i.e. sensitivity, resolution, and signal to noise ratio) improves following electrode gap decrease as the result (Acar and Shkel, 2008). These allegations will be proved in section 6. In sections 3 and 4, a new composite adaptive controller (CAC), for a single-axis 2-DOF MEMS vibratory gyro with seven uncertain parameters, is also proposed in order to overcome fabrication problematic issues, low accuracy in modelling and pivotal faults with open loop design. It also obtains desired sinusoidal vibrations with non-destructive operational amplitudes and frequencies along two orthogonal axes. The uncertain parameters are the stiffness and damping factors as well as rotation rate. The benefit is that the whole system appears more swift and sharp in estimation of all discussed unknown parameters and robust being subjected into much more severe external fixed disturbance, all in comparison to ASMC (Fei, 2012). Justified parameter estimation in the suggested scheme, however, is because of persistently excitation condition (PEC). PEC is brought about by unequal drive excitation frequencies in two vibration mechanisms, likewise ASMC. The comparative simulation study between ASMC and CAC verifies that the latter is capable of demonstrating more accuracy, considerable identification pace and sharpness, and even more robustness, especially in parameter estimation. As depicted on Fig. 7, the contributing control scheme of CAC includes two major bodies; a conventional model reference adaptive controller (MRAC) and a self-tuning regulator (STR) (Ranjbar et al. 2018). The first part plays the role to realize a thorough faultless tracking of distinct sinusoidal vibrations along drive and sense directions and the second estimates the rotation rate. It owns an intrinsic tunable speed and robustness in parameter alteration track. Indeed, two parameter update laws are embedded in the system; the first one vouches for the system stability and the second guarantees right estimation of unknown gyroscopic parameters. The technique is established upon external drive force matrix decomposition and error dynamical equation matrix factorization as well. The error dynamical equation is decomposed into parameters' estimation error vector and regressor (trajectory) matrix because of decomposition of external drive or control force vector. The result is deemed as a prediction error and attempts are done to make a cost function minimized. The cost index betokens exponential prediction error growth. The minimized cost yields the parameters' update law equation where the regressor matrix is involved. The system

parameters update law appears as a function of trajectories because the matrix itself is a function of accessible trajectories. Increase in richness of the regressor matrix is so important since it boosts excitation of more modes and guarantees PEC and estimation of the parameters such as angular velocity as the main result. It is worthwhile notifying that trajectory data are given by electronic measuring circuits and the reference model. The delicate point which mandates one's focus to be maintained is that ASMC, depicted on Fig. 8, loses pace and accuracy due to operation upon smooth transient switching function instead of $\text{sgn}(s)$ to overcome lumped uncertainty and disturbance, in order to assuage chattering consequences. Notably, CAC shows extraordinary disturbance rejection in comparison to ASMC. The variable, s , is the sliding surface.

The article is structured as following. A single-axis 2-DOF MEMS vibratory gyroscope model is intuitively conversed and represented in section 2. Persuasive simulation yields and comparison with ASMC are put forth. In section 3 and 4, CAC and estimator are devised and adjusted. The simulation results are illustrated in section 5. The conceptual analysis of modifying contribution in gyroscopic structure is discussed in section 6. Final outcomes as well as some future attractive research fields are presented in section 7.

2. MODEL REVIEW AND PRINCIPLES OF OPERATION

As shown on Fig. 1, the structure is thought up in such a way that the seismic mass is capable of vibrating along two major perpendicular axes entitled x and y . The described structure is chiefly made up of two vibratory mechanisms (Acar and Shkel, 2008); drive vibrator and sense one; the x vibrational mechanism involves the proof mass, the suspension structure that allows the seismic mass to vibrate merely along the x direction, stationary/moving x comb drive electrostatic actuation electrodes and stationary/moving x comb differential capacitance sense electrodes, and so does the y vibrator (Acar and Shkel, 2008; Ranjbar et al., 2013, 2014). The vibration along the sense axis betokens the rotation rate which is going to be measured (Acar and Shkel, 2008). Rotation rate measurement in MEMS vibratory gyroscope is based upon displacement measurement brought about by the resulting Coriolis force. The so called "Coriolis force induction" principle is presented to clarify the MEMS vibratory gyroscopic mechanism (Ranjbar et al., 2014; John and Vinay, 2006).

Note that the forces are applied by two blocks of electronic circuits, numbered 8 and 9, connected to the x and y actuation electrodes which are signed with V_x , $-V_x$, V_y and $-V_y$ on Fig. 1. Additionally, the signals proportional

to the proof mass constrained displacements, velocities and accelerations along the x and y axes are respectively measured by two blocks of trans-impedance amplification circuits which are numbered with 10 and 11 on Fig. 1. More explanation and details about the electro-mechanical transduction embedded mechanisms are provided in Section 6. It is necessary notifying that dynamical model of the novel conceptual design, more explained in Section 6, does not differ from the previous ones in (Acar and Shkel, 2008; John and Vinay, 2006). Before obtaining the proof mass equations, it is emphasized that presumptions come in subsequent order; first off, the gyro is subjected into rotation and transition. Secondly, the substrate has the non-accelerated transitive movement and constant rotary speed. Furthermore, the centripetal forces become so partial and the gyro rotates just around the z direction in such a way that the Coriolis force is produced merely along x and y directions (Acar and Shkel, 2008). Presume $V = V_x + V_y$ as the vector in the rotating frame, x - y . Time derivative of V in the inertial frame, X - Y , turns

$$\left(\frac{d\vec{V}}{dt}\right)_{XY} = \left(\frac{d\vec{V}}{dt}\right)_{xy} + \vec{\omega} \times \vec{V}, \quad (1)$$

where ω is the rotation rate of the rotating frame x - y . $\left(\frac{d\vec{V}}{dt}\right)_{XY}$ and $\left(\frac{d\vec{V}}{dt}\right)_{xy}$ are respectively time-derivatives of the vector \vec{V} (its mapping) in the rotating frame and (its mapping) in the inertial frame (Meriam and Kraige, 2012), as illustrated on Fig. 2(b).

The rotating frame is attached to the substrate on which the seismic mass is kept in suspension as illustrated in Fig. 2. Before obtaining the seismic mass equations, the following symbols are introduced regarding Fig. 2(c); r_A as the position vector of the seismic mass relative to the inertial coordinate system A (X - Y), r_B as the position vector of the seismic mass relative to the rotating coordinate system B (x - y) and θ as an orientation vector of the rotating coordinate system B relative to the inertial one A. Ω is the rotation rate of the rotating coordinate system B ($\Omega = \dot{\theta}$) and R is the position vector of the gyro's substrate (rotating coordinate system B). The dynamical equation will be obtained via describing the position vector of the seismic mass in two parts; one term with respect to the rotating coordinate system and the other with respect to the inertial one so;

$$\begin{aligned} r_A &= R + r_B \xrightarrow{d/dt} \dot{r}_A = \dot{R} + \dot{r}_B + \dot{\theta} \times r_B \xrightarrow{d/dt} \\ \ddot{r}_A &= \ddot{R} + \ddot{r}_B + \dot{\theta} \times \dot{r}_B + \ddot{\theta} \times r_B + \dot{\theta} \times (\dot{r}_B + \dot{\theta} \times r_B) \Rightarrow \\ \vec{a}_A &= \vec{A} + \vec{\Omega} \times \vec{r}_B + \vec{\Omega} \times (\vec{\Omega} \times \vec{r}_B) + 2\vec{\Omega} \times \vec{v}_B + \vec{a}_B. \end{aligned} \quad (2)$$

\vec{A} is the transitive acceleration of the gyro substrate. Ultimate obtained term, \vec{a}_A , is the acceleration of the seismic mass relative to the inertial frame A (Acar and Shkel, 2008). In (2), the term, $2\vec{\Omega} \times \vec{v}_B$, is the Coriolis acceleration which is the major function that transforms rotation rate of the rotating reference frame B into an imaginary inertial force Acar and Shkel (2008). Finally, the whole external force influencing over the seismic mass is attained by (3) assuming the transitive acceleration to be inconsiderable;

$$\vec{F}_{ext} = m\vec{\Omega} \times \vec{r}_B + m\vec{\Omega} \times (\vec{\Omega} \times \vec{r}_B) + 2m\vec{\Omega} \times \vec{v}_B + m\vec{a}_A, \quad (3)$$

$$\vec{F}_{ext} = m(\dot{\Omega}_y z - \dot{\Omega}_z y + \Omega_y \Omega_x y - \Omega_z^2 x - \Omega_z \Omega_x z + 2\Omega_y \dot{z} - 2\Omega_z \dot{y} + \ddot{x})\vec{i} + m(\dot{\Omega}_z x - \dot{\Omega}_x z + \Omega_z \Omega_y z - \Omega_z^2 y - \Omega_x^2 y + 2\Omega_z \dot{x} - 2\Omega_x \dot{z} + \ddot{y})\vec{j} + m(\dot{\Omega}_x y - \dot{\Omega}_y x + \Omega_x \Omega_z x$$

$$+ \Omega_x \Omega_y x - \Omega_x^2 z - \Omega_y^2 z + \Omega_y \Omega_z y + 2\Omega_x \dot{y} - 2\Omega_y \dot{x} + \ddot{z})\vec{k}. \quad (4)$$

It is supposed that the gyro's substrate rotates just around the z direction with a fixed rotation rate. Consequently, $\Omega_x = 0$, $\dot{\Omega}_x = 0$, $\Omega_y = 0$ and $\dot{\Omega}_y = 0$. It will not be exaggerative that the seismic mass hardly diverges out of the parallel plane with the gyro's substrate, resulting in no movement along the z direction - $z = \dot{z} = \ddot{z} = 0$. For rotation rates at frequencies lower than the gyro operational frequency, the term Ω_z^2 becomes partial Acar and Shkel (2008); the centripetal forces are negligible as emphasized before. These presumptions simplify the long Eq. (4):

$$\vec{F}_{ext} = m(-2\Omega_z \dot{y} + \ddot{x})\vec{i} + m(2\Omega_z \dot{x} + \ddot{y})\vec{j}. \quad (5)$$

From another aspect, it may be stated that

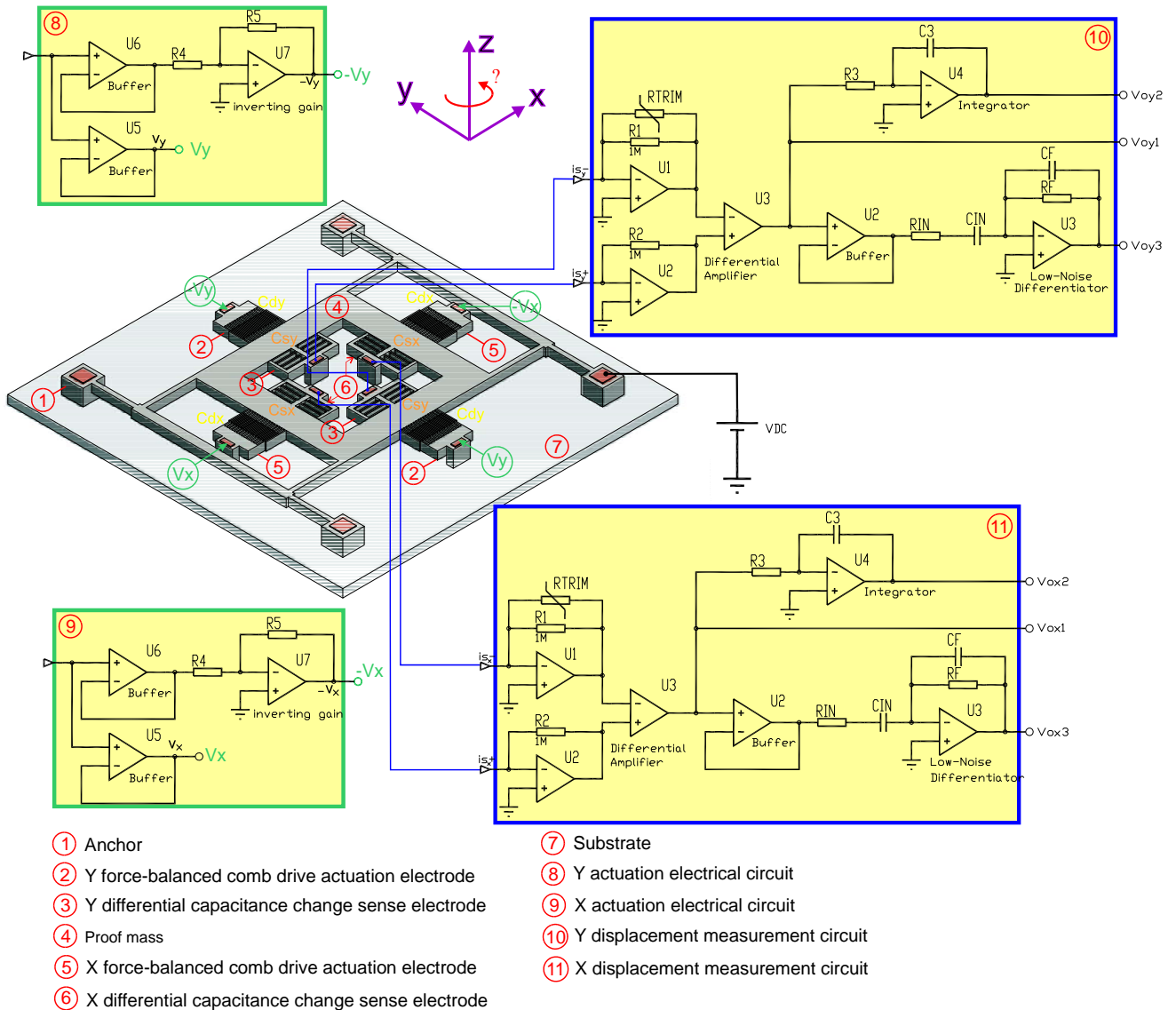


Fig. 1. Physical construction of the MEMS vibratory gyro which is equipped with force balanced actuators and differential capacitance sensory bridges together simultaneously.

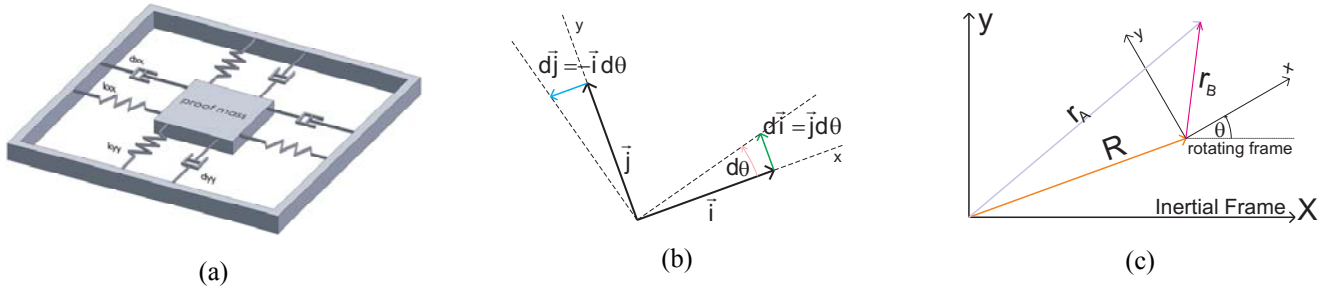


Fig. 2. (a) Gyro lumped model (b) Derivative of rotating vector (c) Gyro's table is virtually connected to the rotating coordinate system.

$$\vec{F}_{ext} = (u_x - d_x \dot{x} - k_x x) \vec{i} + (u_y - d_y \dot{y} - k_y y) \vec{j} \quad (6)$$

where u_x and u_y are control forces along the two directions.

The resistant elastic and damping forces are considered against the moving forces; u_x , and u_y . The following equations will be obtained regarding (5) and (6):

$$u_x + 2m\Omega_z \dot{y} = d_x \dot{x} + k_x x + m\ddot{x} \quad (7)$$

$$u_y - 2m\Omega_z \dot{x} = d_y \dot{y} + k_y y + m\ddot{y} \quad (8)$$

Geometric abnormalities unavoidably decrease stability and rotation rate measurement accuracy. Indeed, separate mode vibrations cross-couple in practice. In other terms, coupling exists between the mentioned resistant coercions of the drive and sense modes due to geometrical abnormalities. Cross stiffness and damping factors might be taken into account in subsequent formulation (Rashed and Momeni, 2007):

$$m\ddot{x} = u_x - d_{xx} \dot{x} - d_{xy} \dot{y} - k_{xx} x - k_{xy} y + 2m\Omega_z \dot{y} \quad (9)$$

$$m\ddot{y} = u_y - d_{yy} \dot{y} - d_{yx} \dot{x} - k_{yy} y - k_{yx} x - 2m\Omega_z \dot{x} \quad (10)$$

3. CAC DESIGN

Now, a CAC is designed which guarantees faultless tracking of desired trajectories and is capable of rotation rate estimation. As it is seen on Fig. 7, CAC is made up of two major bodies (Controller and STR); the first subsystem is the adaptive Lyapunov-based model reference controller which is responsible for tracking desired trajectory perfectly in such a way that the whole system stabilizes. The second is a self-tuning regulator which plays the role of estimator to make a correct measurement of uncertain parameters, particularly the rotation rate. The suggested CAC is designed in such a way that it has the quadrature error compensated in order to obtain desiderated sinusoidal vibrations with suitably defined amplitudes and frequencies along the two directions. It intensively results in so swift and precise angular velocity estimation, being subjected into aggravating exogenous disturbance.

Gyroscopic dynamics may be restated so that it would be similar to a 2-DOF robot equation Fei (2012). Dividing (9) and (10), by m and defining vectors, $q = [x \ y]^T$, $u = [u_x \ u_y]^T$, and matrices as:

$$\Omega = \begin{bmatrix} 0 & -\Omega_z \\ \Omega_z & 0 \end{bmatrix}, D = \begin{bmatrix} d_{xx} & d_{xy} \\ d_{yx} & d_{yy} \end{bmatrix}, K = \begin{bmatrix} k_{xx} & k_{xy} \\ k_{yx} & k_{yy} \end{bmatrix}, \quad (11)$$

the gyro dynamics would be subsequently reconsidered;

$$\ddot{q} + D\dot{q} / m + Kq / m + 2\Omega\dot{q} = u / m. \quad (12)$$

It is worth transforming equations into non-dimensional ones for simulation goals. Regarding resonance frequency of drive and sense mode vibration mechanism as ω_0 and assuming external applied frequencies to be ω_d and ω_s , one may take into account non-dimensional time t' as $t' = \omega_0 t$ and $dt' / \omega_0 = dt$ as the result. Equation (12) is a two-rowed vector equation. Supplanting t with t' / ω_0 and dividing first and second rows respectively by the reference displacement x_0 and y_0 then completely by ω_0^2 yield

$$\begin{aligned} & \frac{d^2 q(t' / \omega_0)}{q_0 dt'^2} + \frac{1}{m\omega_0 q_0} D \frac{dq(t' / \omega_0)}{dt'} + \frac{1}{m\omega_0^2 q_0} Kq(t' / \omega_0) \\ & = \frac{1}{m\omega_0^2 q_0} u(t' / \omega_0) - \frac{1}{\omega_0 q_0} 2\Omega \frac{dq(t' / \omega_0)}{dt'}. \end{aligned} \quad (13)$$

Defining vector variables and matrix parameters as following: $\ddot{q}' = d^2 q(t' / \omega_0) / q_0 dt'^2$, $\dot{q}' = dq(t' / \omega_0) / q_0 dt'$, $q' = q(t' / \omega_0) / q_0$, $u' = u(t' / \omega_0) / m\omega_0^2 q_0$, $D' = (1 / m\omega_0) D$, $K' = (1 / m\omega_0^2) K$ and $\Omega' = (1 / \omega_0) \Omega$, the plant equation appears as:

$$\ddot{q}' + D'\dot{q}' + K'q' = u' - 2\Omega'\dot{q}' \quad (14)$$

or the subsequent one by crossing out the prime symbol:

$$\ddot{q} + D\dot{q} + Kq = u - 2\Omega\dot{q}. \quad (15)$$

At this stage, a CAC is designed to achieve thorough tracking

of the seismic mass and rotation rate estimation. Perfect tracking is obtained exploiting an MRAC (Model Reference Adaptive Controller) and gyro parameters are measured by an STR. The non-dimensional gyroscopic dynamics is reconsidered as

$$\ddot{q} + (D + 2\Omega)\dot{q} + Kq = T, \quad (16)$$

where T is the control force-vector. The dynamical equation can be recast by

$$M\ddot{q} + V + K_l = T \quad (17)$$

where, $M = \begin{bmatrix} M_{11} & M_{12} \\ M_{21} & M_{22} \end{bmatrix} = \begin{bmatrix} 1 & 0 \\ 0 & 1 \end{bmatrix}$, $T = \begin{bmatrix} \tau_1 \\ \tau_2 \end{bmatrix} = u = \begin{bmatrix} u_1 \\ u_2 \end{bmatrix}$, and

$$V = \begin{bmatrix} d_{xx}\dot{q}_1 + d_{xy}\dot{q}_2 - 2\Omega_z\dot{q}_2 \\ d_{yx}\dot{q}_1 + 2\Omega_z\dot{q}_1 + d_{yy}\dot{q}_2 \end{bmatrix}, K_l = \begin{bmatrix} n_{xx}q_1 + n_{xy}q_2 \\ n_{yx}q_1 + n_{yy}q_2 \end{bmatrix} \quad (18)$$

This plant is constructed on the simulation block 1 on Fig. 7. It is presumed that $d_{xy} = d_{yx}$, and $\eta_{xy} = \eta_{yx}$. Were this supposition not considered, number of uncertain parameters could merely grow without losing generosity and any problem imposition on final solution.

The control force vector can be factorized into product of regressor matrix and parameters' vector so the dynamics is reconsidered and (16) would be converted into (19);

$$T = W(s)P(t) = W(q, \dot{q}, \ddot{q})P(t). \quad (19)$$

Thus, $W(s)$ and $P(t)$ are obtained by the next equations:

$$W(s) = \begin{bmatrix} \ddot{q}_1 & 0 & \dot{q}_2 & -\dot{q}_2 & q_2 & \dot{q}_1 & q_1 & 0 & 0 \\ 0 & \ddot{q}_2 & \dot{q}_1 & \dot{q}_1 & q_1 & 0 & 0 & \dot{q}_2 & q_2 \end{bmatrix} \quad (20)$$

$$P(t) = [M_{11} \quad M_{22} \quad d_{xy} \quad 2\Omega_z \quad n_{xy} \quad d_{xx} \quad n_{xx} \quad d_{yy} \quad n_{yy}] \quad (21)$$

If the uncertainties are neglected, control input, v , and control law, T , are going to be designed subsequently in such a way that they vouch for tracking error zero convergence and system stability.

$$v = \ddot{q}_d + K_v\dot{\tilde{q}} + K_p\tilde{q} \quad (22)$$

$$T = Mv + V + K_l \quad (23)$$

In (22) and (23), $\tilde{q} = q_d - q$, is the tracking error. K_v and K_p are fixed matrices defined by $K_v = \text{diag}\{\lambda_1^2, \lambda_2^2\}$ and $K_p = \text{diag}\{2\lambda_1, 2\lambda_2\}$ where λ_1 and λ_2 are positive adjustment constants. If this control law is superseded in the system dynamics, it would bring about a Hurwitz tracking error dynamics;

$$M\ddot{q} + V + K_l = T \xrightarrow{T=Mv+V+K_l} \ddot{q} + K_v\dot{\tilde{q}} + K_p\tilde{q} = 0.$$

On the other hand, there is uncertainty in parameters, hence the control law modification;

$$T = \hat{M} [\ddot{q}_d + K_v\dot{\tilde{q}} + K_p\tilde{q}] + \hat{V} + \hat{K}_l. \quad (24)$$

Supplanting the latter control law in (17) would yield the next tracking error dynamics:

$$M\ddot{q} + V + K_l = \hat{M} [\ddot{q}_d + K_v\dot{\tilde{q}} + K_p\tilde{q}] + \hat{V} + \hat{K}_l. \quad (25)$$

Equations (22) and (24) are constructed within blocks 3 and 4 on Fig. 7. Regarding $M = \tilde{M} + \hat{M}$, $V = \tilde{V} + \hat{V}$ and $K_l = \tilde{K}_l + \hat{K}_l$, and supplanting them with the corresponding terms at the left side of (25) would lead to

$$\tilde{M}\ddot{q} + \tilde{V} + \tilde{K}_l = \hat{M} [\ddot{q} + K_v\dot{\tilde{q}} + K_p\tilde{q}]. \quad (26)$$

Equation (26) is multiplied by the inverse of the so-called "estimated mass matrix", \hat{M}^{-1} . Even though \hat{M} equals to $M (M = I_2)$, the multiplication is carried out as an inspiratory solution for such problematic an issue while grams of the seismic mass is undetermined. Nevertheless, the article is concerned with a mass-defined gyroscope.

$$\ddot{q} + K_v\dot{\tilde{q}} + K_p\tilde{q} = \hat{M}^{-1} [\tilde{M}\ddot{q} + \tilde{V} + \tilde{K}_l] \quad (27)$$

Equation (27) changes into (28) regarding (17) and (19);

$$\ddot{q} + K_v\dot{\tilde{q}} + K_p\tilde{q} = \hat{M}^{-1} W(q, \dot{q}, \ddot{q}) \tilde{P}(t). \quad (28)$$

Bringing the latter mass presumption into the mind, (28) is converted into

$$\ddot{q} + K_v\dot{\tilde{q}} + K_p\tilde{q} = W(q, \dot{q}, \ddot{q}) \tilde{P}(t). \quad (29)$$

The tracking error dynamics could be stated in terms of product of trajectory regressor matrix and uncertain parameter estimation error vector. A state space model may be depicted considering the tracking error dynamics. The proof mass movement along the two vibrational-trajectory axes are regarded as state variables, hence adoption of state vector by $X^T = [x_1 \mid x_2]_{1 \times 4} = [\tilde{q} \mid \dot{\tilde{q}}]_{1 \times 4} = [\tilde{q}_1 \quad \tilde{q}_2 \quad \dot{\tilde{q}}_1 \quad \dot{\tilde{q}}_2]_{1 \times 4}$.

Its time-derivative can be stated as following:

$$\dot{x}_1 = x_2 \quad (30)$$

$$\dot{x}_2 = -K_p x_1 - K_v x_2 + W\tilde{P} \quad (31)$$

Hence, the state space model is given in subsequent terms:

$$\dot{X} = AX + BU \quad (32)$$

where $X = [x_1 \mid x_2]^T = [\tilde{q} \mid \dot{\tilde{q}}]^T$, $U = W\tilde{P}$, and

$$A = \begin{bmatrix} 0_{2 \times 2} & I_2 \\ -K_p & -K_v \end{bmatrix} \text{ and } B = \begin{bmatrix} 0_{2 \times 2} \\ I_2 \end{bmatrix}. \quad (33)$$

System output can be deemed as the following combined error vector which includes weighted tracking errors of displacement and velocity. It is noteworthy that $\alpha > 0$, $\psi_j > 0$ and $\Psi_{2 \times 2} = \text{diag}\{\psi_1, \psi_2\}$.

$$Y = \alpha \begin{bmatrix} \dot{\tilde{q}}_1 + \psi_1 \tilde{q}_1 \\ \dot{\tilde{q}}_2 + \psi_2 \tilde{q}_2 \end{bmatrix} = \alpha \begin{bmatrix} \dot{\tilde{q}}_1 \\ \dot{\tilde{q}}_2 \end{bmatrix} + \alpha \begin{bmatrix} \psi_1 & 0 \\ 0 & \psi_2 \end{bmatrix} \begin{bmatrix} \tilde{q}_1 \\ \tilde{q}_2 \end{bmatrix} \\ = [\alpha \Psi_{2 \times 2} \quad \alpha I_2] X \quad (34)$$

Therefore, output is announced by the observer matrix C and the state space vector (seen at the bottom of Fig. 7 next to block numbered 6):

$$Y = CX \text{ and } C = \alpha [\Psi_{2 \times 2} \quad I_2]. \quad (35)$$

As constructed within block 6 on Fig. 7, the output is defined by positive weighting factors of error and its time-derivative ($\alpha > 0$, $\psi_j > 0$). Maximum degree of time-derivative of the error is one. A is a strictly stable matrix (Slotine and Li, 1991). Equation (36) gives the input-output transfer function matrix;

$$Y(s) = \text{diag} \left\{ \alpha(s + \psi_1) / (s + \lambda_1)^2, \alpha(s + \psi_2) / (s + \lambda_2)^2 \right\}. \quad (36)$$

It is strictly positive real (SPR) due to 4 conditions of SPR functions (Slotine and Li, 1991). $\{A, B\}$ is a controllable pair because controllability matrix rank is full ($[B \mid AB \mid A^2B \mid A^3B]_{4 \times 8} = 4$). It is worth being noticed that $\det[B \mid AB]_{4 \times 4} = 1 \neq 0$, hence a controllable linear time-independent system depiction. In the description, input-output transfer function appears SPR. Consequently, necessities of the Kalman-Yakovovich Lemma are provided (Slotine and Li, 1991), and it could be affirmed that symmetric positive definite matrices, P and Q , lay in such a way that

$$A^T P + PA = -Q \text{ and } PB = C^T. \quad (37)$$

The subsequent Lyapunov candidate, which is a function of tracking and parameter estimation errors, is selected as

$$V(X, \tilde{P}) = X^T P X + \tilde{P}^T \Gamma^{-1} \tilde{P} \quad (38)$$

where $\Gamma_{9 \times 9}$ presents a symmetric positive definite matrix. Time-derivative of the function is obtained in (39).

$$\dot{V}(X, \tilde{P}) = \dot{X}^T P X + X^T P \dot{X} + 2\tilde{P}^T \Gamma^{-1} \dot{\tilde{P}} \quad (39)$$

\dot{V} is made simple regarding the state space model;

$$\dot{V} = (AX + BU)^T P X + X^T P (AX + BU) + 2\tilde{P}^T \Gamma^{-1} \dot{\tilde{P}} \quad (40)$$

$$\dot{V} = X^T (A^T P + PA) X + U^T B^T P X + X^T P B U + 2\tilde{P}^T \Gamma^{-1} \dot{\tilde{P}}. \quad (41)$$

With regard to (37) and the scalar terms of $U^T B^T P X$ and $X^T P B U$, (41) changes to

$$\dot{V}(X, \tilde{P}) = -X^T Q X + 2U^T B^T P X + 2\tilde{P}^T \Gamma^{-1} \dot{\tilde{P}}. \quad (42)$$

Summation of sign-indefinite terms are zeroed stabilizing the system, considering (37) and (43);

$$\dot{\tilde{P}} = -\Gamma W^T B^T P X = -\Gamma W^T C X = -\Gamma W^T Y. \quad (43)$$

With regard to parameter consistency or slow variation, (43) is expressed in another way;

$$\dot{\hat{P}} = \Gamma W^T C X = \Gamma W^T Y. \quad (44)$$

Equation (44) is the parameters' update law which is constructed in block 5 on Fig. 7. The matrix, $W(q, \dot{q}, \ddot{q})$, is obtained through linear parameterization of the exogenous driving force vector into the regressor matrix and the uncertain parameter vector. The matrix is produced in block 9 on Fig. 7. It should be brought into one's mind that

$$\hat{P}(t) = [1 \quad 1 \quad \hat{d}_{xy} \quad 2\hat{\Omega}_z \quad \hat{n}_{xy} \quad \hat{d}_{xx} \quad \hat{n}_{xx} \quad \hat{d}_{yy} \quad \hat{n}_{yy}] \quad (45)$$

and $\lambda_1 = \lambda_2 = 10$ as well as $\Gamma = 150I_9$. Equation (37) and equality of Q to $-I_2$ are all exploited for P determination;

$$P = \begin{bmatrix} 2.625 & 0 & 0.005 & 0 \\ 0 & 2.625 & 0 & 0.005 \\ 0.005 & 0 & 0.0253 & 0 \\ 0 & 0.005 & 0 & 0.0253 \end{bmatrix} \quad (46)$$

Considering (37), matrix C is equal to

$$C = \begin{bmatrix} 0.005 & 0 & 0.0253 & 0 \\ 0 & 0.005 & 0 & 0.0253 \end{bmatrix} \quad (47)$$

Regarding (35), $\alpha = 0.0253$, $\psi_1 = \psi_2 = 5 / 25.3$.

4. LEAST MEAN SQUARE ESTIMATION SCHEME BASED UPON BOUNDED EXPONENTIAL FORGETTING FACTOR

Here, an estimator will be devised to identify uncertain parameters, particularly the rotation rate. The following output prediction error might be defined;

$$e_p = \hat{y} - y. \quad (48)$$

The exogenous driving forces over the gyro are regarded as output. The output will be forestalled by the prediction system. As it was proved, the output could be factorized into

the regressor matrix and the uncertain parameters' vector, hence a new restatement of the prediction error:

$$e_p = W(s)\hat{P}(t) - W(s)P(t) = W(s)\tilde{P}(t). \quad (49)$$

The prediction error is generated via the red line part, numbered with 11 on Fig. 7 as well as block 10. The following cost function is proposed as the accumulated prediction error index;

$$J = \int_0^t \|e_p(t)\|^2 ds = \int_0^t \|W(s)\hat{P}(t) - y(s)\|^2 ds. \quad (50)$$

The cost function minimization yields zeroing $\partial J / \partial \hat{P}$. It is demonstrated by Slotine and Li (1991) that the estimator, which is expressed by (51) and (52), minimizes the suggested index. Equations (51) and (52) betoken the parameters and gain update laws respectively;

$$\dot{\hat{P}} = -G(t)W^T(s)e_p, \quad (51)$$

$$\dot{\hat{G}} = -G(t)W^T(s)W(s)G(t). \quad (52)$$

The estimator shows inertial. It requires a huge memory for data storage as well. It becomes incapable of tracking the time-dependant parameters as data accumulates with identification advancement. While PEC gets fragile, explosive gain corruption and annoying sensitivity become apparent. However, the major benefit of the system is a fine noise filtration and disturbance rejection which could be contemplated as robustness to some extent. Assuaging spoiling effect of piled-up data and compelling the estimation mechanism to be farther swift as well as improving time-dependant parameter tracking competency, the least mean square estimator with bounded exponential forgetting factor is suggested. The subsequent cost function is proposed as the lumped prediction error index (Slotine and Li, 1991);

$$J = \int_0^t e^{-\int_s^t \lambda(r)dr} \|W(s)\hat{P}(t) - y(s)\|^2 ds. \quad (53)$$

Minimization of the cost function again yields in zeroing $\partial J / \partial \hat{P}$. Estimator-descriptive Eq. (54) and (55), respectively as the parameters and gain update laws, minimize the suggested cost function;

$$\dot{\hat{P}} = -G(t)W^T(s)e_p \quad (54)$$

$$\dot{\hat{G}} = \lambda(t)G(t) - G(t)W^T(s)W(s)G(t) \quad (55)$$

The two recent equations are implemented in blocks 7 and 8 of Fig. 7 and so are the Eq. (51) and (52).

Were λ set to zero, the simple inertial estimator would be applied. It is not competent of following time-dependant parameters. There would be too much sensitivity when PEC

became fragile with time progression. Were λ a nonzero fixed value, there would be a least square estimator with constant forgetting factor. It somehow would be a fine solution for the problem of huge memory requirement and sensitivity issue when PEC grew fragile during the time, because of eruptive gain increase ($\lim_{t \rightarrow \infty} \|G(t)\| = \infty$). Avoiding the gain corruption, λ is adopted time-dependant in such a way that it will converge to zero if PEC turns fragile and it will increase resulting in data forgetting intensification if PEC is fostered. $\lambda(t)$ is given by Slotine and Li (1991);

$$\lambda(t) = \lambda_0(1 - \|G(t)\|/K_0). \quad (56)$$

λ_0 is a desired fixed value. K_0 is calculated by the supremum of the gain matrix (Slotine and Li, 1991);

$$K_0 = \sup_{t>0} \|G(t)\|. \quad (57)$$

These fixed values are adjusted by trial and error through simulation. There is another equation between the gain and trajectory regressor matrices in the least mean square estimator with bounded exponential forgetting factor (Slotine and Li, 1991);

$$G^{-1}(t) = G^{-1}(0)e^{-\int_0^t \lambda(r)dr} + \int_0^t e^{-\int_0^r \lambda(r)dr} W^T(s)W(s) ds. \quad (58)$$

According to (58), $\|G\|$ betokens PEC. When PEC loses its intensity, $\|G\|$ will grow and $\lambda(t)$ would diminish considering (56) as the result. This extenuates data forgetting and hampers gain explosion. While PEC intensifies, $\|G\|$ will step down and $\lambda(t)$ will grow contemplating (56). It yields farther data forgetting and a swift estimator as an important consequence. Selecting greater amounts for λ_0 causes more data forgetting and enhances time-dependant parameter tracking competency; however, it causes much more oscillatory deviations in parameter estimation. It mandates a trade-off to choose between time-dependant parameter tracking pace and oscillations in parameter estimation. The proposed CAC involves two major parts: MRAC and STR. See Fig. 8 and 7.

Table 1. Major parameters of the single-axis 2-DOF MEMS vibratory gyro.

Parameter	Nominal value	Parameter	Nominal value
m	$1.8 \times 10^{-7} \text{ Kg}$	d_{xx}	$1.8 \times 10^{-6} \text{ Ns / m}$
k_{xx}	63.955 N / m	d_{yy}	$1.8 \times 10^{-6} \text{ Ns / m}$
k_{yy}	95.92 N / m	d_{xy}	$3.6 \times 10^{-7} \text{ Ns / m}$
k_{xy}	12.779 N / m	Ω_z	200 rad / s

5. SIMULATION RESULTS

Simulation schemes of the novel proposed ASMC and CAC are depicted on Fig. 8 and 7. Blocks of STR and controller, on Fig. 7, are separated with two different background colors – pale orange and yellow respectively. The proposed CAC control design is verified through simulation utilizing parameter values in Table 1. It is put under operation being prone to abnormal conditions such as being susceptible to seven undetermined parameters and also aggravating fixed disturbance. Initial values of parameters are 90% of the real ones. The gyro is vulnerable to a rotation rate of 200 rad/sec. As it could be seen on Fig. 3(a), thorough tracking is attained. Not only is the tracking performance convincing and do the combined tracking and prediction errors tend to zero, but also all the parameters, including angular velocity, are measured and have tended to their real values as depicted on Fig. 4(a), 5(a) and 6(a). The proposed control-measurement design is more rapid and much more precise than ASMC in (Fei, 2012). ASMC is simulated resulting in depictions of Fig. 3(b), 4(b), 5(b), and 6(b). Figure 3(b) illustrates ASMC tracking performance while the three others, including 4(b), 5(b) and 6(b), are displaying parameter convergence achievement. One may make a comparison between CAC and ASMC correspondingly observing Fig. 3(a) and 3(b). He also keeps up with the judgment comparing 4(a), 5(a), 6(a) respectively with 4(b), 5(b) and 6(b). The consequent judgment is on behalf of absolute preference of the proposed CAC to ASMC from aspects of identification speed, preciseness and considerable tracking performance as well. Figure 3 demonstrates that the tracking error converges nearly to zero in about 0.0005 sec at CAC while it converges to zero in 0.07 sec at ASMC. As demonstrated and analyzable on Fig. 4(a) and 4(b), the damping factors of d_{xx} , d_{yy} and d_{xy} converge to their real values in about 0.0003 sec at the CAC system whereas they get close to the physical values in about 0.07 sec or 0.08 sec in the ASMC system. Likewise, as depicted and comparable on Fig. 5(a) and 5(b), stiffness factors of k_{xx} , k_{yy} and k_{xy} converge to their real values in about 0.0003 sec at CAC while they get close to the actual values in about 0.07 sec in ASMC. Again, shown and measurable on Fig. 6(a) and 6(b), the angular velocity has been estimated in about 0.0003 sec with ultra high precision at the CAC scheme that the angular velocity has got close to the real value of 200 rad/sec in 0.07 sec with unsatisfactory precision in the ASMC scheme; it is about 168 or 172 rad/sec. All these comparisons confirm superiority of CAC to ASMC in speed and accuracy. The CAC system performs at least 233 times faster than the ASMC system. This superiority draws one's attention while we notice that the disturbance imposed

on the input force channels of the CAC system are respectively 45 and 54 while they are about 0.18 in the ASMC system - which means imposing a more exacerbating condition on our CAC in comparison to the ASMC system. See Fig. 3(a) and 3(b) and compare the disturbance. Notably, all the other simulation conditions such as parameter values, noise, etc. are quite alike for both CAC and ASMC. On the figures related to the convergence of parameters in both CAC and ASMC, the result of the division of the values signed with green circles by the values flagged by the red circles is about 1.11 which represents a 10% divergence of the real values of parameters from nominal values – the considered parametric uncertainty in the system dynamics. If the green circle-flagged values and the red ones are assumed to be v_g and v_r , then $v_g / v_r = 1.11$, and

$$\text{Divergence}(\%) = (v_g - v_r) \times 100 / v_g \simeq 10\%. \quad (59)$$

ASMC Lyapunov function is firstly considered as

$$V(s, \tilde{p}_s) = s^T s / 2 + \tilde{p}_s^T \Gamma_s^{-1} \tilde{p}_s / 2 \quad (60)$$

where s , \tilde{p}_s , Γ_s are respectively sliding surface, parameters' estimation error and symmetric positive definite matrix. The adaptive parameters' update law, (61), is responsible for stabilizing the Lyapunov candidate. Furthermore, PEC contributes to true parameter convergence because of the regressor matrix richness influenced by inequality of operational stimulating frequencies.

$$\dot{\hat{p}} = -\Gamma_s W^T s \quad (61)$$

In Fig. 8, it is calculated in block 4. $\hat{\theta}$ is the symbol of \hat{p} which is parameter estimation vector. W is the regressor matrix which mandates the reference model to provide necessary richness. It would appear in time-derivative of the sliding surface trying to extrude out a vector of uncertain parameters. The control law in (62) comes with the latter equations compelling the system to track the desired trajectories thoroughly and faultlessly. It is constructed in block 5 on Fig. 8.

$$u = W \hat{p} - \sum_{i=1}^2 \omega_i^2 / \omega_0^2 q_i - \sum_{i=1}^2 \lambda_i (q_i - q_{i_d}) - \sum_{i=1}^2 \eta_i \text{sgn}(s_i) \quad (62)$$

η_i is a positive fixed value which should be larger than lumped uncertainty norm including unknown spring and damping forces, and fixed disturbance if all η_i are contemplated equal. Another delicate point is that supplanting $\text{sat}(s_i)$ with $\tanh(s_i)$ or $\text{sgn}(s_i)$, to diminish chattering phenomenon, undesirably influences parameter estimation and successful perfect tracking.

6. CONTRIBUTING CONCEPTUAL SCHEMATIC DESIGN MODIFICATION

As displayed on Fig. 1, two parallel plate variable area capacitor pairs (comb drive structure) along either x or y axis can be distinguished. Electrostatic actuation force is obtained by (63) for a variable-area capacitor structure presuming capacitance of each companion of the capacitor pair along the x axis as $C_{dx}(t)$ while the proof mass has no displacement (Acar and Shkel, 2008).

$$F = 0.5V_e^2 \partial C / \partial x \tag{63}$$

V_e is the electrical potential across x stretch. x is the displacement along x axis and x_0 is the initial length which is shared between two plates and forms an effective capacitance area. For a balanced comb drive structure in each

companion of the pair, when the proof mass moves, the lengths will be $x_0 + x$ and $x_0 - x$ with respect to each companion. The two capacitances are presented by (64) presuming d and t to be respectively as finger separation and thickness or height.

$$C_{dx}^{\pm}(t) = \epsilon_0 (x_0 \pm x(t))t / d \tag{64}$$

Each moving finger plate connected to the proof mass is surrounded by two stationary lateral finger plates yielding changes in two areas and doubling the electrostatic actuation force as the result. Contemplating (63) and (64), the balanced force over the moving finger is achieved by (65) ($V_e = V_{DCx}^{\pm} = V_{DC} \pm V_x$)

$$F_x = 2 \times \frac{1}{2} \left(\frac{\partial C_{dx}^+}{\partial x} V_{DCx}^+{}^2 + \frac{\partial C_{dx}^-}{\partial x} V_{DCx}^-{}^2 \right) = 4\epsilon_0 t V_{DC} V_x / d \tag{65}$$

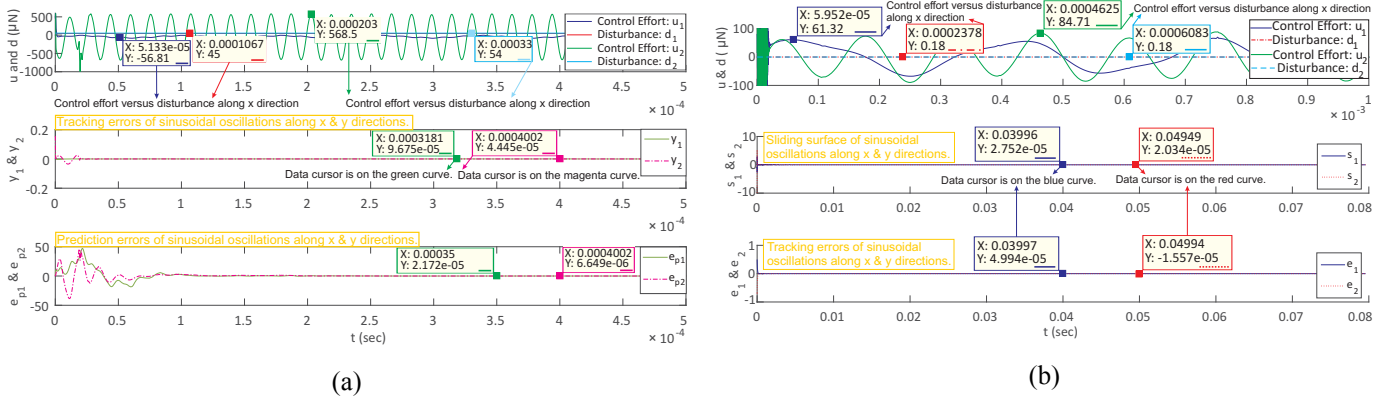


Fig. 3. Tracking performance: (a) CAC (b) ASMC. CAC is more rapid and accurate regarding data cursors and time axis scale.

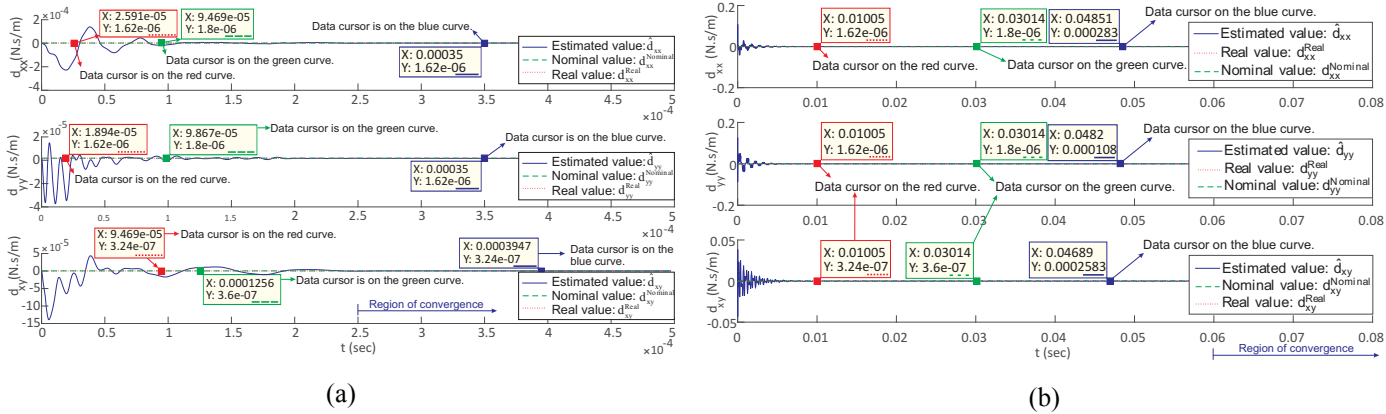


Fig. 4. Parameter convergence associated with damping and cross-damping factors in the designed CAC and ASMC; as it is seen, the estimated damping factors converge to their real values more rapidly and precisely in the CAC in comparison with the ASMC (0.07/0.0003≈233 times faster).

For a comb drive structure including N moving fingers connected to each lateral side of the seismic mass and two sets of $N+1$ fixed fingers attached to the respective lateral parts of the substrate along the x axis, as displayed on Fig. 1, the whole balanced force equals to

$$F_{xt} = 4N\epsilon_0 t V_{DC} V_x / d. \tag{66}$$

It is noteworthy that F_{xt} functions the variable voltage, which is applied as the control effort, in a linear manner.

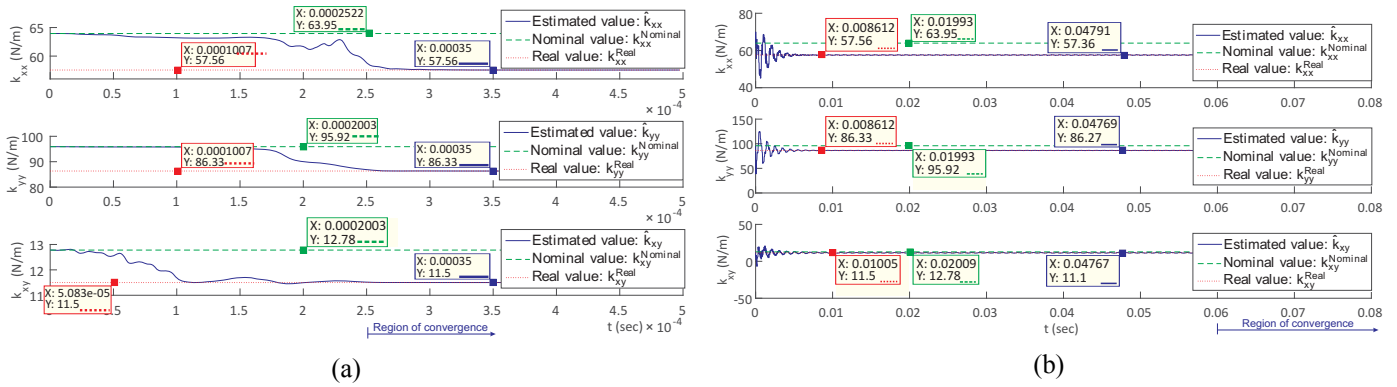


Fig. 5. Parameter convergence associated with stiffness and cross-stiffness factors in the designed CAC and ASMC; as it is seen, the estimated damping factors converge to their real values more rapidly and precisely in the CAC in comparison with the ASMC.

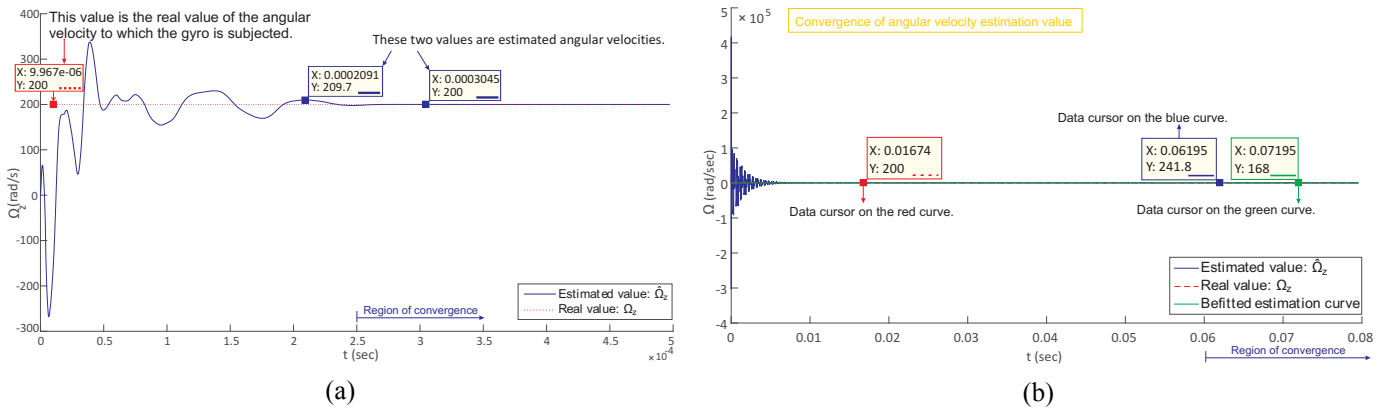


Fig. 6. Parameter convergence in the designed CAC and ASMC; as it is seen, the angular velocity gets converged to real value of 200 (rad/sec) in the CAC faster and more accurate in comparison with the ASMC.

As displayed on Fig. 1, the two differential variable-gap capacitor pairs along either x or y axis are distinguished. Capacitance of each companion of the capacitor pair along the x axis are presumed to be $C_{sx}(t)$ while the mass has no displacement. For a displacement along the x axis, the fingers, which are parallel to the y axis and connected to the mass, get close to one set of fixed fingers connected to the substrate resulting in capacitance increase and get far from the other fixed set yielding capacitance decrease. Reasonably, capacitance of each companion of the x capacitor pair is expressed by (67).

$$C_{sx}^{\pm}(t) = C_{sx}(t) \pm \Delta C_{sx} \quad (67)$$

Logically, a differential capacitive bridge is had constituted. Take into account electrical charge and current of each capacitor companion respectively as q_{sx}^+ , q_{sx}^- , i_{sx}^+ and i_{sx}^- . Suppose G_{U3} to be the gain of differential amplifier in Fig. 1 and presume R_{trim} to get adjusted in order to make compensation for resistor tolerances of R_1 and again R_1 as well. Therefore, V_{ox1} could be affirmed in subsequent mathematics;

$$\begin{aligned} V_{ox1} &= G_{U3}(i_{sx}^+ R_1 - i_{sx}^- R_1) = G_{U3} R_1 (\dot{q}_{sx}^+ - \dot{q}_{sx}^-) \\ &= G_{U3} R_1 V_{DC} \frac{d}{dt} \{ (C_{sx}(t) + \Delta C_{sx}) - (C_{sx}(t) - \Delta C_{sx}) \} \rightarrow \\ V_{ox1} &= 2G_{U3} R_1 V_{DC} \frac{d(\Delta C_{sx})}{dt} = 2G_{U3} R_1 V_{DC} \frac{\partial \Delta C_{sx}}{\partial x} \dot{x}. \end{aligned} \quad (68)$$

The differential capacitance for an electrode, including N fingers on each side, could be stated by (69) regarding L as the length of the fingers Acar and Shkel (2008).

$$\Delta C = C_{sx}^+ - C_{sx}^- \approx 2N \epsilon_0 t L x / d^2. \quad (69)$$

Regarding (68) and (69), V_{ox1} and V_{ox3} are calculated as:

$$V_{ox1} = G_{U3} R_1 V_{DC} 4N \epsilon_0 t L \dot{x} / d^2, \quad (70)$$

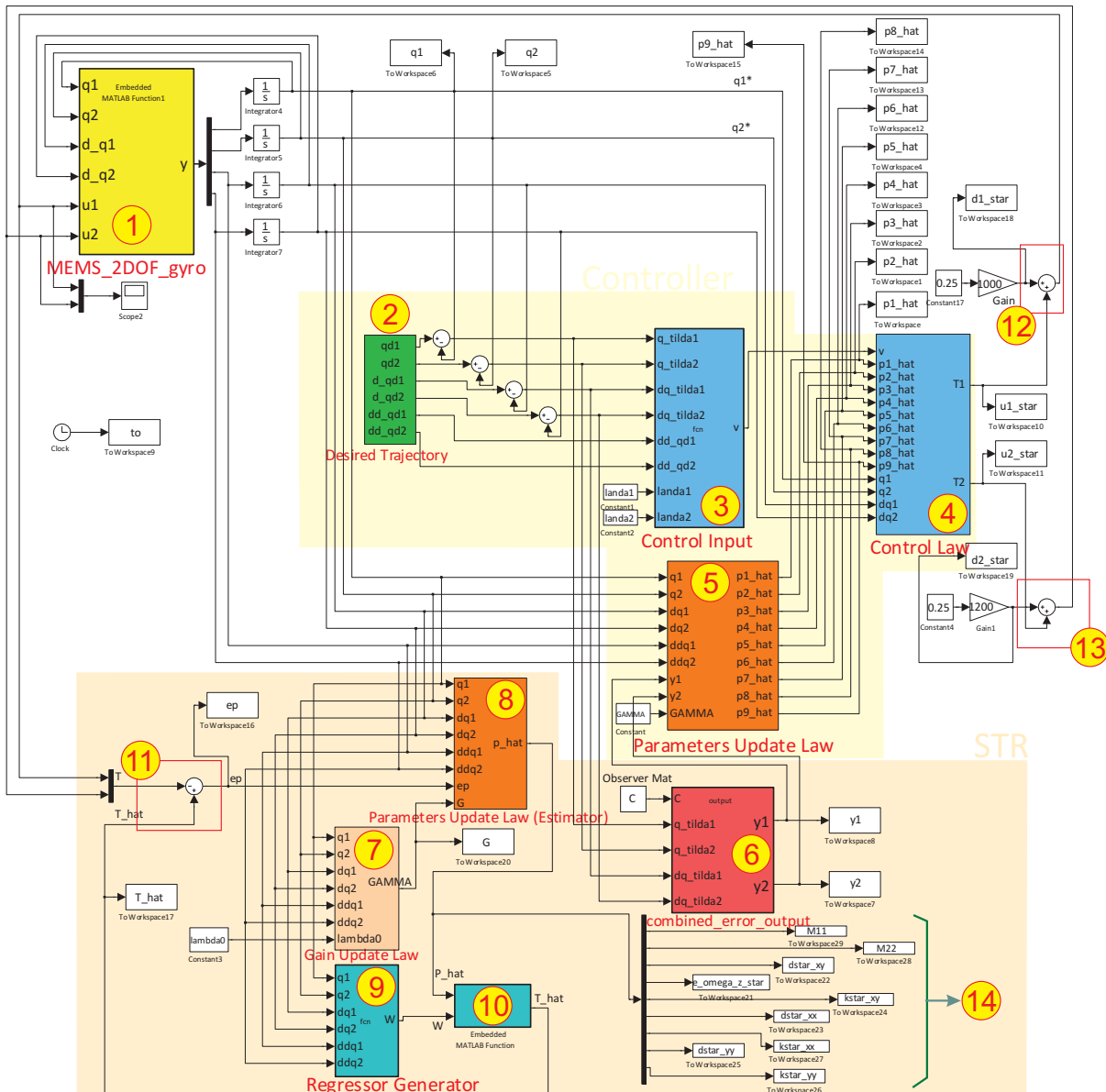
$$V_{ox3} = \dot{V}_{ox1} = G_{U3} R_1 V_{DC} 4N \epsilon_0 t L \ddot{x} / d^2. \quad (71)$$

Hence, V_{ox1} and V_{ox3} are approximated by velocity and acceleration linear functions. Likewise, along the y axis:

$$F_{yt} = 4N \epsilon_0 t V_{DC} V_y / d, \quad (72)$$

$$V_{oy1} = G_{U3} R_1 V_{DC} 4N \epsilon_0 t L \dot{y} / d^2, \quad (73)$$

$$V_{oy3} = \dot{V}_{oy1} = G_{U3} R_1 V_{DC} 4N \epsilon_0 t L \ddot{y} / d^2. \quad (74)$$



- 1 Plant
- 2 This block generates the desired trajectory.
- 3 This one refers to Eq. (22).
- 4 Equation (24) is established by this block.
- 5 The block calculates integration of Eq. (44) and is in charge of stability.
- 6 This one gives out the combined error which is defined by Eq. (35)
- 7 This item may refer to integration of Eq. (52) or (55) to put matrix $G(t)$ at the access.
- 8 The block could represent integration of Eq. (51) or (54) and is in charge of parameter estimation.
- 9 This block produces the regressor matrix according to Eq. (22).
- 10 This multiplies the regressor matrix by the parameter estimation vector.
- 11 This part demonstrates the prediction error calculation statement.
- 12 & 13 At these two parts, the disturbance is matched and added to the forces.
- 14 This item refers to the estimated parameters.

Fig. 7. Simulation Scheme of CAC.

Driving voltages of the sensor, V_x and V_y , ought to be applied in such a way that $u_x = F_{xt}$ and $u_y = F_{yt}$. It should not be concealed out of mind that u_x and u_y are control efforts. It is significant to notice that the seismic mass acceleration along the x and y directions should be exploited because the regressor matrix, $W(q, \dot{q}, \ddot{q})$, functions the linear accelerations. Therefore, the velocity variables which are

available should be differentiated and they are the mass velocity along the x and y axes. The conventional differentiator op-amp circuitry or an inductor could be applied for the purpose but it brings about serious noisy measurements! Not only could the modified differentiating op-amp circuit in Fig. 9 be utilized on the ground of the distinct gyro operating frequency and band-pass filtration of the measuring signal adjusting the cut-off frequencies in the

accessorial circuits, but also the STR would effectively suppress measurement noise regarding its inertial dynamics. See Fig 1. Another solution might be proposed to avoid second time-derivative of the mass displacement. It is

filtration of linear parameterized equation of forces, $T = W(q, \dot{q}, \ddot{q})P(t)$, via a stable first-order filter and exploitation of convolving integral transforming \ddot{q} into \dot{q} (Slotine and Li, 1991).

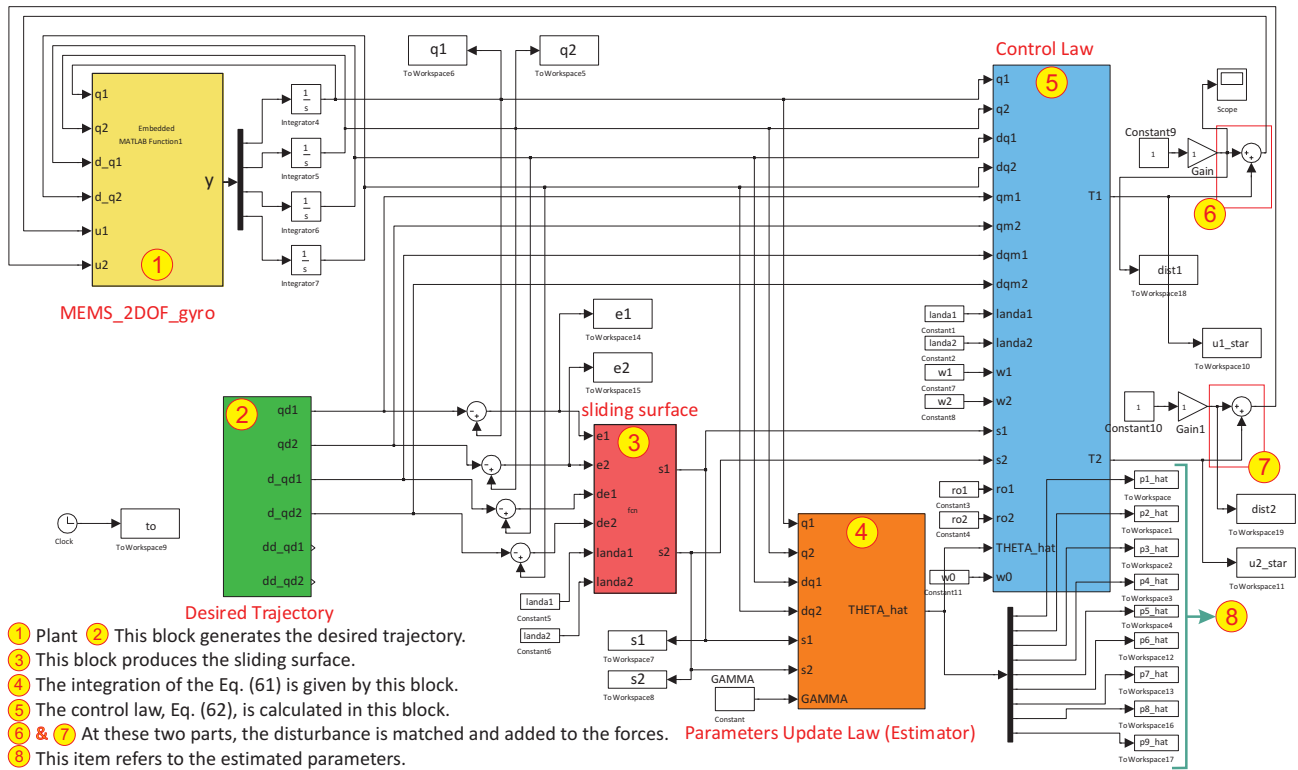


Fig. 8. Simulation Scheme of ASMC.

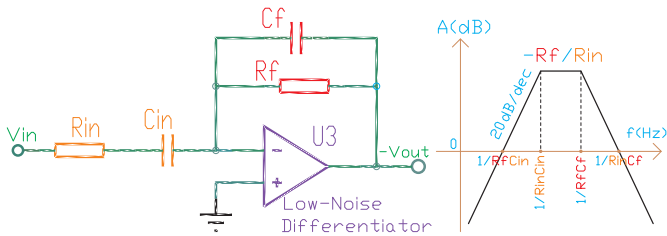


Fig. 9. Frequency response of the modified differentiator to reduce the measurement noise.

7. CONCLUSION AND FUTURE WORK

By and large, sinusoidal vibration guarantee, along the drive and sense directions with desirable operational amplitudes and frequencies for more accurate rotation rate measurement, appears so crucial an issue in the MEMS 2-DOF single axis gyro application. The topic gets controversial considering unavoidable parameter uncertainty, aniso-elasticity and aniso-damping caused by imperfection in fabrication process. Consequently, proposal of competent control schemes will be so beneficial and contributing to compensation of quadrature error. The suggested CAC vouches for the sinusoidal vibrations with desirable amplitudes and frequencies along the perpendicular directions, each orthogonal to the rotation axis. Stimulating the system with two unequal driving

frequencies, the designed STR embedded at the composite scheme, appears swift in estimation of angular velocity and other gyroscopic parameters. Furthermore, the whole control scheme takes advantage of adjustable speed and intrinsic structural robustness through tuning of multiple constant parameters; not only is the suggested CAC perfectly involved in successful tracking and parameter estimation, but also it functions speedily and precisely in a more robust manner, imposing absolute superiority to ASMC. The implementation proposal individually gets derived of landmark stability, linear manipulation and detection capacitive mechanisms resulting in controllability and observability of the gyroscopic system. Nonetheless, more investigative numerical design and model validation and modification could be put into one’s prospective for a serious research field. The model parameters are merely presumed to equal to some values, approximately similar to the actual operational status. Naturally, it is suggested to make a quantitative assessment of the model using a finite element software for verification of the model parameters such as stiffness and damping factors, and the mass as well, running a static simulation. Functionality of the angular velocity sensor susceptible to high frequency control effort signal ought to be inspected implementing a thorough software modal analysis;

however, dynamic simulative sensor investigation might be a hard and time-consuming task. Linear parametrization of the applied control effort to assuage the undesirable effect of linear acceleration terms in the control law could be another challenging issue to boost the performance of the controlling system.

REFERENCES

- Acar, C. and Shkel, A. (2008). *MEMS Vibratory Gyroscopes; Structural Approaches to Improve Robustness*. Springer, 1 edition.
- Devaraj, J.A. (2015). Adaptive particle swarm optimization based system identification and internal model sliding mode controller for mass ow system. *Journal of Control Engineering & Applied Informatics (CEAI)*, 17(4), 3-13.
- Dong, L. and Avanesian, D. (2009). Drive-mode control for vibrational MEMS gyroscopes. *IEEE Transactions on Industrial Electronics*, 56(4), 956-963.
- Fei, J. and Batur, C. (2009). A novel adaptive sliding mode control with application to MEMS gyroscope. *ISA Transactions*, 48(1), 73-78.
- Fei, J., Juan, W., and Li, T. (2011). An adaptive fuzzy control approach for the robust tracking of a MEMS gyroscope sensor. *International Journal of Advanced Robotic Systems*, 8, 125-133.
- Fei, J. (ed.) (2012). *Advanced control design of MEMS vibratory gyroscope*. Nova Science Publishers.
- Fei, J., Xin, M., and Juan, W. (2013). Adaptive fuzzy sliding mode control using adaptive sliding gain for mems gyroscope. *Transactions of the Institute of Measurement & Control*, 35(4), 551-558.
- Jiang, C., Xue, L., Chang, H., Yuan, G., and Yuan, W. (2012). Signal processing of MEMS gyroscope arrays to improve accuracy using a 1st order markov for rate signal modeling. *Sensors*, 12(2), 1720.
- John, J.D. and Vinay, T. (2006). Novel concept of a single-mass adaptively controlled tri-axial angular rate sensor. *IEEE Sensors Journal*, 6(3), 588-595.
- Juan, W. and Fei, J. (2013). Adaptive fuzzy approach for non-linearity compensation in mems gyroscope. *Transactions of the Institute of Measurement & Control*, 35(8), 1008-1015.
- Li, W., Lan, T., and Lin, W. (2010). The nonlinear control of the drive axis for a vibrating MEMS gyroscope. *In 5th International Conf. on Computer Science & Education (ICCSE)*, 1198-1203.
- Meriam, L.J. and Kraige, L.G. (2012). *Engineering mechanics; dynamics*. John Wiley & Sons, New Jersey, 7 edition.
- Raman, J., Cretu, E., Rombouts, P., and Weyten, L. (2009). A closed-loop digitally controlled MEMS gyroscope with unconstrained sigma-delta force-feedback. *IEEE Sensors Journal*, 9(3), 297-305.
- Ranjbar, E., Suratgar, A.A., and Khatamie, S. (2014). Functionality and modeling of a 3-DOF tri-axial MEMS vibratory gyroscope. *In Proceedings of the First International Conf. on MEMS & Microfabrication*.
- Rashed, R. and Momeni, H. (2007). System modeling of MEMS gyroscopes. *In Proceedings of the 15th Mediterranean Conference on Control & Automation*, 1-6. Athens, Greece.
- Rossomando, F.G., Soria, C., and Carelli, R. (2014). Sliding mode control for trajectory tracking of a non-holonomic mobile robot using adaptive neural networks. *Journal of Control Engineering & Applied Informatics (CEAI)*, 16(1), 12-21.
- Saif, M., Ebrahimi, B., and Vali, M. (2011). Terminal sliding mode control of z-axis MEMS gyroscope with observer based rotation rate estimation. *In Proceedings of the 2011 American Control Conf.*, 3483-3489.
- Salah, M.H., McIntyre, M.L., Dawson, D.M., Wagner, J.R., and Tatlicioglu, E. (2010). Sensing of the time-varying angular rate for MEMS z-axis gyroscopes. *Mechatronics*, 20(6), 720-727.
- Sefriti, S., Boumhidi, J., Naoual, R., and Boumhidi, I. (2012). Adaptive neural network sliding mode control for electrically- driven robot manipulators. *Journal of Control Engineering & Applied Informatics (CEAI)*, 14(4), 27-32.
- Slotine, E. and Li, W. (1991). *Applied Nonlinear Control*. Prentice Hall, New Jersey.
- Wang, X., Li, H., Xia, G., Liu, B., and Yang, B. (2011). Research and experiment on the drive frequency control of the MEMS gyroscope. *In Second International Conf. on Mechanic Automation & Control Eng. (MACE)*, 547-550.
- Wu, D. and Fei, J. (2016). Adaptive neural sliding control of MEMS gyroscope with robust feedback compensator. *Transactions of the Institute of Measurement & Control*, 38(4), 414-424.
- Yuan, D., Ma, X., Liu, Y., Shang, Z., and Yan, S. (2016). Statistical modeling of random walk errors for triaxial rate gyros. *IEEE Transactions on Instrumentation & Measurement*, 65(2), 286-296.
- Ranjbar, E. and Suratgar, A. A. (2018). A Composite Adaptive Controller Design for 3-DOF MEMS Vibratory Gyroscopes Capable of Measuring Angular Velocity. *Iranian Journal of Science and Technology, Transactions of Electrical Engineering*, 1-22.
- Ranjbar, E. and Suratgar, A. A. (2013). Design of an adaptive controller for a 2-DOF MEMS vibratory gyroscope to obtain perfect tracking and angular velocity estimation with noise, disturbance and parameter variation analysis. *The 3rd International Conference on Control, Instrumentation, and Automation, Dec 2013*, 224-23.